Competition for iron shapes metabolic antagonism between Bacillus subtilis and Pseudomonas marginalis

Lyng, M.; Jørgensen, J.P.B.; Schostag, M.D.; Jarmusch, S.A.; Aguilar, D.K.C.; Lozano-Andrade, C.N.; Kovács, A.T.

The ISME Journal, 2024, **18(1)**, 1–13
https://doi.org/10.1093/ismejo/wrad001
Original Article

Competition for iron shapes metabolic antagonism between *Bacillus subtilis* and *Pseudomonas marginalis*

Mark Lyng[1], Johan P.B. Jørgensen[1], Morten D. Schostag[2], Scott A. Jarmusch[3], Diana K.C. Aguilar[1], Carlos N. Lozano-Andrade[1], Ákos T. Kovács[1,4,*]

[1]Bacterial Interactions and Evolution Group, DTU Bioengineering, Technical University of Denmark, Kgs Lyngby 2800, Denmark
[2]Bacterial Ecophysiology & Biotechnology, DTU Bioengineering, Technical University of Denmark, Kgs Lyngby 2800, Denmark
[3]Natural Product Discovery, DTU Bioengineering, Technical University of Denmark, Kgs Lyngby 2800, Denmark
[4]Institute of Biology Leiden, Leiden University, Leiden 2333 BE, The Netherlands

*Corresponding author: Ákos T. Kovács, Institute of Biology Leiden, Leiden University, Sylviusweg 72, Leiden 2333 BE, The Netherlands. Email: a.t.kovacs@biology.leidenuniv.nl

Abstract

Siderophores have long been implicated in sociomicrobiology as determinants of bacterial interrelations. For plant-associated genera, like *Bacillus* and *Pseudomonas*, siderophores are well known for their biocontrol functions. Here, we explored the functional role of the *Bacillus subtilis* siderophore bacillibactin (BB) in an antagonistic interaction with *Pseudomonas marginalis*. The presence of BB strongly influenced the outcome of the interaction in an iron-dependent manner. The BB producer *B. subtilis* restricts colony spreading of *P. marginalis* by repressing the transcription of histidine kinase-encoding gene *gacS*, thereby abolishing production of secondary metabolites such as pyoverdine and viscosin. By contrast, lack of BB restricted *B. subtilis* colony growth. To explore the specificity of the antagonism, we cocultured *B. subtilis* with a collection of fluorescent *Pseudomonas* spp. and found that the *Bacillus–Pseudomonas* interaction is conserved, expanding our understanding of the interplay between two of the most well-studied genera of soil bacteria.

Keywords: iron, siderophore, bacillibactin, Bacillus subtilis, Pseudomonas, GacSA

Introduction

Interactions between bacteria are of huge relevance to how microbial ecology can be manipulated for biotechnological benefit. In natural environments, bioavailable iron is often scarce and because it is an essential mineral to virtually all life, many organisms have evolved to scavenge iron using high-affinity metal chelators [1]. Metal chelators are a main driver of antagonism between microorganisms both in sequestering metal ions from competing organisms and through bioactive toxicity, directly inhibiting or even killing competitors [2, 3].

The catecholate siderophore bacillibactin (BB) produced by members of the *Bacillus* genus is an example of an iron chelator that performs multiple functions. In *Bacillus subtilis*, it is the main iron acquisition metabolite with high affinity for ferric iron, Fe(III) [4]. BB is synthesized through a nonribosomal peptide synthetase pathway encoded by the *dhbA-F* operon and is exported to acquire Fe(III) before being taken up again by the FeuABC-YusV ABC transporter system [5-8]. Once intracellular, BB-Fe is hydrolysed by BesA to release iron ions for use in enzymatic reactions and in transcriptional regulation through the ferric uptake regulator Fur [7].

The *dhbA-F* operon also plays an essential role in *Bacillus* biofilm formation. The Δ*dhbA* mutant lacks dehydrogenation of (2S,3S)-2,3-dihydroxy-2,3-dihydrobenzoate to 2,3-dihydroxybenzoate (DHB) and therefore is unable to produce pellicle biofilms in the biofilm-promoting-defined medium MSgg due to an inability to perform extracellular electron transport with ferric iron captured by DHB [9]. Additionally, BB from *Bacillus amyloliquefaciens* has even been suggested to exhibit direct bioactivity against the plant pathogen *Pseudomonas syringae* pv. *tomato*, though without direct experimental evidence [10], and recent studies have demonstrated the antibacterial properties of BB isomers against *Pseudomonas aeruginosa* [11, 12].

Bacillus and *Pseudomonas* are bacterial genera with high environmental impacts. They are environmentally ubiquitous and often coisolated, especially within the context of crops. Here, they function as biostimulants and biocontrol agents, but also, in the case of *Pseudomonas*, as phytopathogens [13]. Both genera contain members capable of producing bioactive natural products that antagonize competing microbes [14-16], and both can alter the local microbiome [17, 18]. Such abilities have immense implications in areas such as agriculture, where microbiome composition is consistently correlated with plant health and disease outcome [19, 20], and therefore, it is considered as an environmentally friendly agricultural practice that lowers the utilization of chemical pesticides.

Pairwise interactions between bacilli and pseudomonads might therefore play a crucial role in determining plant growth, health, and local microbiome composition. Studies investigating such pairwise interactions are revealing more detail, outlining the molecular mechanisms, and determining the degree to which interactions and their effector molecules are conserved [21-25]. However, despite these advances, the large bioactive potential

Received 25 October 2023. **Accepted:** 3 November 2023

of *Bacillus* and *Pseudomonas* makes mapping the overarching interaction mechanisms challenging, and a consensus has not been reached on the general interactions between members of these two genera. Some studies investigated the role of iron and siderophores, identifying pyoverdine (Pvd) and pyochelin from *Pseudomonas* as informational cues for *Bacillus velezensis* [21], and pulcherriminic acid produced by *B. subtilis* as an iron sequestering agent in interactions with *Pseudomonas protegens* [26].

Here, we investigated the functional role of *B. subtilis* BB in antagonizing *Pseudomonas*. Using a macrocolony competition assay, we observed that *B. subtilis* DK1042 (hereafter, DK1042) was able to restrict the colony size of *Pseudomonas marginalis* PS92 (hereafter, PS92) but that the disruption of the BB biosynthetic pathway reversed the interaction, resulting in diminished growth of DK1042. By disrupting each gene in the *dhb* operon, we found that products of DhbA-F enzymes can be secreted and shared among *B. subtilis* cells. The interaction depended on iron in the media, but transcriptomic analysis revealed no iron starvation response in cocultures. Instead, the PS92 Gac/Rsm signalling system, herein, Pvd biosynthesis, was strongly downregulated transcriptionally and metabolically when cocultured alongside DK1042. Finally, we found that DK1042 could inhibit several fluorescent *Pseudomonas* spp., all in a BB-dependent manner.

Methods

Culturing

The *B. subtilis* DK1042 (the naturally competent derivative of 3610) and *P. marginalis* PS92 were routinely cultured in lysogeny broth (LB; Lennox, Carl Roth, 10 g/l tryptone, 5 g/l yeast extract, and 5 g/l NaCl), LB supplemented with 1% (v/v) glycerol and 0.1 mM $MnCl_2$ (LBGM), or King's B medium (KB; 20 g/l peptone, 1% glycerol (v/v), 8.1 mM K_2HPO_4, 6.08 mM $MgSO_4{\cdot}7H_2O$) at 30°C. Colonies were grown on media solidified with 1.5% agar (w/v). $FeCl_3$, ammonium ferric citrate, and 2,2′-bipyridine (BPD) were added to autoclaved agar at varying concentrations. Antibiotics were added in the following final concentrations: 50 μg/ml gentamycin (Gm), 100 μg/ml ampicillin (Amp), 5 μg/ml chloramphenicol (Cm), and 10 μg/ml Kanamycin (Km).

Pairwise interactions on agar

DK1042 and PS92 were routinely spotted 5 mm apart on agar surfaces using 2 μl of overnight culture adjusted to an optical density at 600 nm (OD_{600}) of 1.0 in appropriate media. Prior to spotting, plates were dried for 30 min in a lateral flow hood and subsequently incubated at 30°C. This experimental setup was employed with all agar competition experiments, also with an in-house collection of fluorescent *Pseudomonas* spp. When spotting mixed cultures, each species was adjusted to an OD_{600} of 1.0, and the two strains were then mixed in equal volumes. For mixed *B. subtilis* cultures, wild-type (WT) and mutant strains were mixed 1:1, 1:10, or 1:100, based on OD_{600}, before spotting 2 μl as detailed above.

Stereomicroscopy

Interactions for stereomicroscopy were assessed using DK1042 carrying *amyE*::$P_{hyperspank}$-*mKate2* and PS92 carrying *attTn7*::*msfGFP*, which constitutively express fluorophores (mKate2 and msfGFP, respectively). Colonies were imaged with a Carl Zeiss Axio Zoom V16 stereomicroscope equipped with a Zeiss CL 9000 LED light source and an AxioCam 503 monochromatic camera (Carl Zeiss, Jena, Germany). The stereoscope was equipped with a PlanApo Z 0.5×/0.125 FWD 114 mm and filter sets 38 HE eGFP (ex: 470/40, em: 525/50) for msfGFP and 63 HE mRFP (ex: 572/25, em: 629/62) for mKate2. Exposure time was optimized for appropriate contrast.

Image processing and analysis were performed using FIJI (2.1.0/1.53f51) [27]. Contrast in fluorescence channels was adjusted identically on a linear scale. Colony area was measured by segmenting the colony of interest using Otsu's algorithm [28] based on fluorescence (msfGFP or mKate2 for *Pseudomonas* or *Bacillus*, respectively).

Viable cell counting

Entire macrocolonies were harvested after 72 h incubation into 1 ml 0.9% NaCl, vortexed with 100 μl glass beads (r = 100 μm) for 10 min, and sonicated with a probe sonicator for 45 s in 1-s pulses (1 s on, 1 s off) at an amplitude of 25%. Homogenized colonies were diluted and spread on LB + 50 μg/ml gm (selecting for PS92) or LB + 5% NaCl (selecting for DK1042 and Δ*dhbA*).

Genetic modification

DK1042 mutants were created through homologous recombination using the *B. subtilis* single gene deletion library [29]. In brief, genomic DNA from a donor *B. subtilis* 168 mutant was extracted using a EURx Bacterial & Yeast Genomic DNA Purification Kit (EURex, Gdansk, Poland) following the manufacturer's instructions, and 100–200 ng genomic DNA was added to DK1042 grown to $OD_{600} \sim 0.5$ in 400 μl at 37°C in competence medium (80 mM K_2HPO_4, 38.2 mM KH_2PO_4, 20 g/l glucose, 3 mM tri-Na citrate, 45 μM ferric NH_4 citrate, 1 g/l casein hydrolysate, 2 g/l K-glutamate, 0.335 μM $MgSO_4{\cdot}7H_2O$, 0.005% [w/v] tryptophan). Cells were incubated with DNA at 37°C for 3 h before 100 μl of the transformation mix was spread onto LB agar supplemented with kanamycin and incubated at 37°C for 16–24 h. Mutants were validated by colony PCR with primers designed to anneal 50–150 bp up- and downstream of the gene of interest (Table S1).

PS92 attTn7::*msfGFP* was constructed by conjugation with pBG42 as described by Zobel *et al.* [30]. In brief, cultures of *Escherichia coli* λ*pir* CC118/pBG42 (donor—Gm^R), *E. coli* HB101/pRK600 (helper, Cm^R), *E. coli* λ*pir* CC118/pTNS2 (transposase-carrying, Amp^R), and PS92 (recipient) were started in LB medium supplemented with appropriate antibiotics and incubated overnight. Each culture was washed thrice in 0.9% NaCl before being mixed equally based on OD_{600}. The mix was spotted onto LB without antibiotics and incubated overnight at 30°C. Resultant colonies were resuspended in 0.9% NaCl and plated on Pseudomonas Isolation Agar (45.03 g/l; Millipore, Burlington, MA, USA) supplemented with Gm to select for positive *Pseudomonas* conjugants.

Mass spectrometry imaging

Pairwise interaction colonies were grown on 10 ml agar plates incubated for 72 h before being excised, dried, and sprayed for matrix-assisted laser desorption ionization-mass spectrometry imaging (MALDI-MSI). Agar was adhered to MALDI IntelliSlides (Bruker, Billerica, Massachusetts, USA) using a 2-Way Glue Pen (Kuretake Co., Ltd, Nara-Shi, Japan). Slides were covered by spraying 1.5 ml of 2,5-dihydrobenzoic acid (40 mg/ml in ACN/MeOH/H_2O [70:25:5, v/v/v]) in a nitrogen atmosphere and dried overnight in a desiccator prior to MSI acquisition. Samples were then subjected to timsTOF flex using a Bruker Daltonik GmbH mass spectrometer for MALDI-MSI acquisition in positive MS scan mode with a 40 μm raster width and a mass range of 100–2000 Da. Calibration was performed using red phosphorus. The settings in timsControl were as follows: Laser: imaging 40 μm, Power Boost 3.0%, scan range 46 μm in the XY interval, laser power

70%; Tune: Funnel 1 RF 300 Vpp, Funnel 2 RF 300 Vpp, Multipole RF 300 Vpp, isCID 0 eV, Deflection Delta 70 V, MALDI plate offset 100 V, quadrupole ion energy 5 eV, quadrupole loss mass 100 m/z, collision energy 10 eV, focus pre TOF transfer time 75 μs, prepulse storage 8 μs. After data acquisition, data were analysed using SCiLS software (version 2021b Pro).

Images were prepared from data normalized to the root-mean square. Images from each m/z value were expanded to be of equal size by adding pixels with NaN values if necessary. Linear scaling of pixel intensity was performed across images displaying the same m/z values. NaN is presented as 0 in the final images.

Liquid chromatography mass spectrometry

B. subtilis DK1042 was inoculated into 20 ml LB in a 100 ml flask and grown overnight. The culture was adjusted to OD_{600} = 1.0, and 1 ml was spread on each of 150 LBGM agar plates and incubated at 30°C for 72 h. Extraction and subsequent liquid chromatography mass spectrometry (LC–MS) analysis were performed as previously described [31]. LC–MS was performed on three independent rounds of culture.

Whole-genome sequencing and genome comparisons

Pseudomonas genomes were sequenced and assembled using a hybrid approach with Oxford Nanopore and Illumina sequencing. From a culture grown in LB overnight, genomic DNA was extracted using a EURx Bacterial & Yeast Genomic DNA Purification Kit following the manufacturer's instructions. Short read library preparation and sequencing were performed at Novogene Co., Ltd on a NovaSeq PE150 platform (Illumina, CA, USA). Long-read library preparation was performed using an SQK-RBK004 Oxford Nanopore Rapid Barcoding kit. Libraries were sequenced on a fresh Oxford Nanopore MinION Mk1B 9.4 flow cell (Oxford Nanopore Technologies, Oxford, UK) for 12 h and base-called simultaneously with Guppy in MinKNOW using the default r941_min_hac_g507 model.

Genomes were assembled using Trycycler (V0.5.3) [32] when the long read sequencing depth was adequate for subsetting or Unicycler (V0.5.0) [33] in all other cases. Adapters were removed using Porechop (0.2.4 https://github.com/rrwick/Porechop), and reads were filtered with Filtlong (V0.2.1 https://github.com/rrwick/Filtlong). Default Trycycler and Unicycler workflows were applied to assemble genomes (see Supplementary Methods for details). Completeness and contamination were assessed using CheckM (V1.1.3) [34], and whole-genome taxonomy was determined with AutoMLST [35] and the TYGS database (V342) [36].

Assembled genomes were annotated with Bakta (V1.6.1) [37], and a gene presence/absence matrix was created with Panaroo (V1.3.2) [38] using its moderate mode and a CD-HIT amino acid identity threshold at 40%. The Panaroo presence/absence matrices were used to create the respective figure.

Transcriptomics

Colonies were collected with a 10 μl loop and placed in RNAse-free screw-cap tubes to sample either the interaction zone (~2 mm into each colony for pairwise interactions) or the entire colony (for monocultures). The collected biomass was solubilized in RNAProtect and frozen in liquid nitrogen before being stored at −80°C prior to RNA purification, for no more than 3 days.

RNA was extracted using a Qiagen RNeasy PowerMicrobiome RNA extraction kit (QIAGEN N.V., Venlo, The Netherlands) via combined bead beating and phenol–chloroform extraction (see Supplementary Methods for details). Ribosomal RNA depletion, library preparation, and sequencing were performed at Novogene Co., Ltd on a NovaSeq PE150 platform.

Read abundances were determined using Kallisto (0.48.0) [39]. The genome of PS92 was annotated with Bakta (V1.6.1) [37], while the genome of *B. subtilis* DK1042 (Acc: CP020102 and CP020103) was retrieved from GenBank. Genomes were converted into a fasta-formatted transcript file with gffread (v0.11.7) [40] then combined into a Kallisto index.

RNA sequencing datasets were trimmed and filtered with FastP, and reads were quantified by mapping every sample to the combined index file (consisting of transcripts from both species), with 100 bootstrap replicates. Differential expression analysis was performed with DESeq2 (v1.34.0) [41] in Rstudio (2022.02.3-b492) [42] running R (4.1.1) [43] with the Tidyverse framework (1.3.1) [44].

Pathway analysis was performed by functionally annotating the transcriptome of each species using eggNOG-mapper V2 (online browser version) with default parameters [45]. Differentially expressed pathways were investigated using KEGG Mapper Reconstruct [46], and manually using the databases Subtiwiki [47] and The *Pseudomonas* Genome Database [48] as references.

Transcriptomic analysis was performed from three independent replicates for each sample.

Statistical analysis and reproducibility

Differences between group means were tested with analysis of variance (ANOVA), coupled with Tukey–Kramer's *post hoc* analysis to determine significantly different means between groups. We adopt df_w to represent the degrees of freedom within groups (i.e. $df_w = n—k$, where n is the total number of samples and k is the total number of groups). One-way repeated measures ANOVA (Fig. 1B) was calculated using the three time points as within-group identifiers. The nonparametric Friedman test was used as data did not satisfy normality requirements as determined with Shapiro–Wilk's normality test. Mean difference between two groups was compared using the nonparametric Wilcoxon rank-sum test. Multiple testing in Fig. 1C was corrected using the Benjamini–Hochberg method. For Figs 2B and C and 5, relative colony sizes of DK1042 and Δ*dhbA* grown on KB for 72 h (Fig. 1B) were included as control groups.

Figure 1B was created from paired groups (time points) of 80 independent datapoints (i.e. 80 pairs of co- and monoculture colonies) from two independent rounds of experiments. Each colony was followed over 72 h, and the subsequent ANOVA was adjusted for paired samples.

All reported *P*-values are adjusted for multiple testing when appropriate.

Results

Bacillibactin is involved in antagonism between DK1042 and PS92

Molina-Santiago and colleagues previously described that on solid KB medium (a growth medium for *Pseudomonas*-produced Pvd detection), DK1042 surrounds and restricts the growth of *Pseudomonas chlororaphis* PCL1606, unlike on various other media used in their experiments [24]. Therefore, we tested a soil-isolated *Pseudomonas* species (designated PS92) and revealed an interaction phenotype comparable to that of PCL1606. Since antagonism was apparent on KB medium, which induces Pvd production in *Pseudomonas*, and not on LB medium (Supplementary Fig. S1A), we hypothesized that siderophores from either DK1042, PS92, or

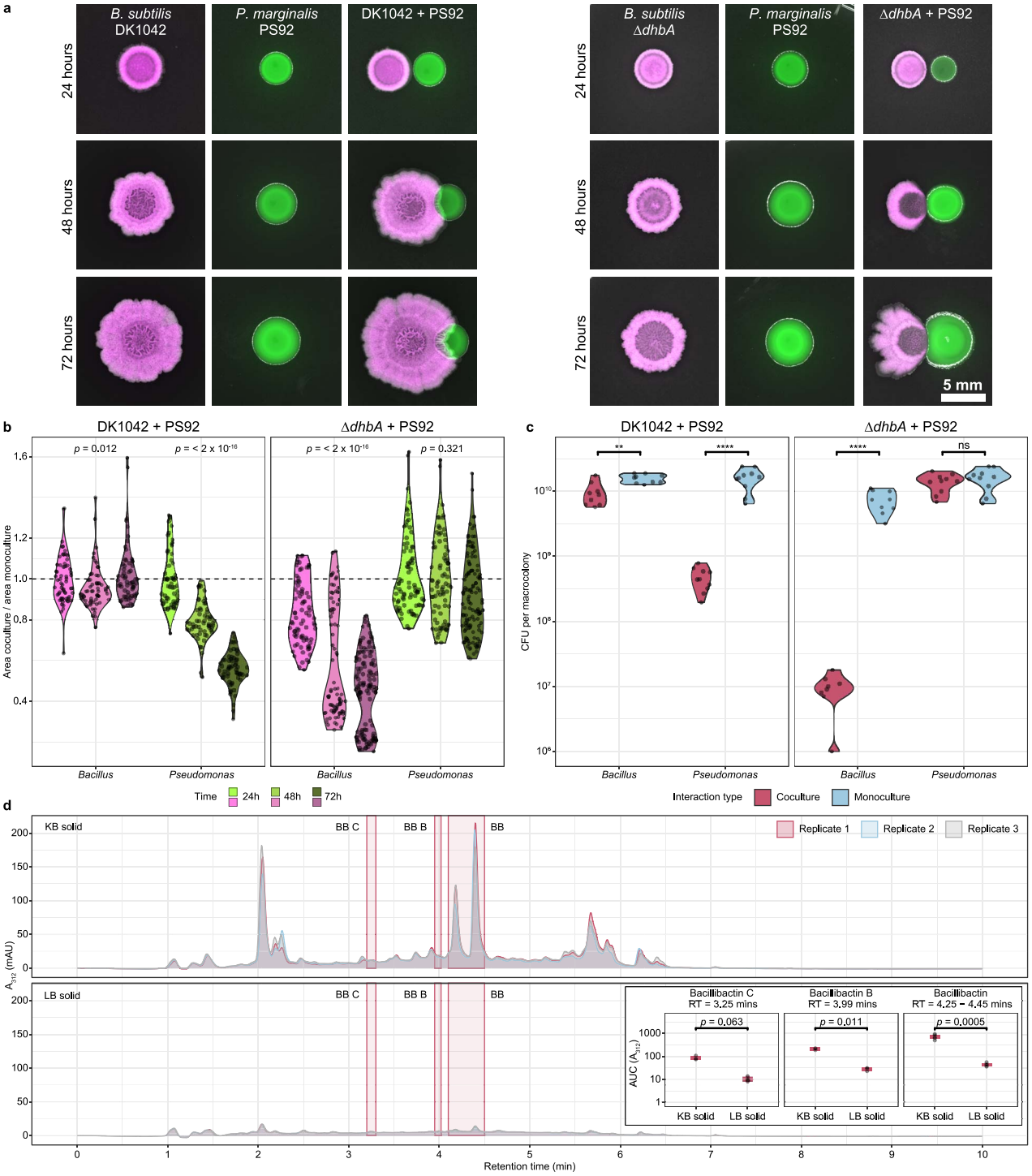

Figure 1. Antagonism is DhbA-dependent; (A) DK1042 (mKate2, false coloured to magenta) and PS92 (msfGFP, false coloured to green) were cocultured on KB agar with 5 mm between colony centres and imaged every 24 h. Scale = 5 mm; (B) coculture colony area was normalized against monoculture colony area and plotted for each partner (x-axis) in the two interactions (facets); the dashed line indicates coculture = monoculture; the *P*-value was calculated by one-way repeated measures ANOVA within groups ($n = 80$ colonies from two independent experiments); (C) colony-forming units were determined from the macrocolonies in coculture and monoculture; significance stars are from Wilcoxon Rank Sum tests ($n = 10$ colonies from two independent experiments; $^{**}P < .01$; $^{****}P < .0001$; ns, not significant; (D) ultra-violet quantification of LC–MS on DK1042 monocultures at $\lambda = 312$ nm; BB and isomers in KB (above) and LB (below); BB, Bacillibactin; BB B, Bacillibactin B; BB C, Bacillibactin C; inset: peak area under the curve (AUC) of BB and isomers in KB and LB; labels are *P*-values from Wilcoxon Rank Sum test ($n = 3$ independent experiments).

both would be involved in this interaction. To evaluate the effect of BB in the interaction between DK1042 and PS92, we cultured fluorescently labelled versions of the two species together in close-proximity macro colonies on solid agar medium. Spots (2 μl) of each culture were placed 5 mm apart and grown at 30°C for 3 days (Fig. 1A and Supplementary Video S1). We compared WT DK1042 and the single gene disruption mutant (Δ*dhbA*) lacking the ability to produce DHB and BB.

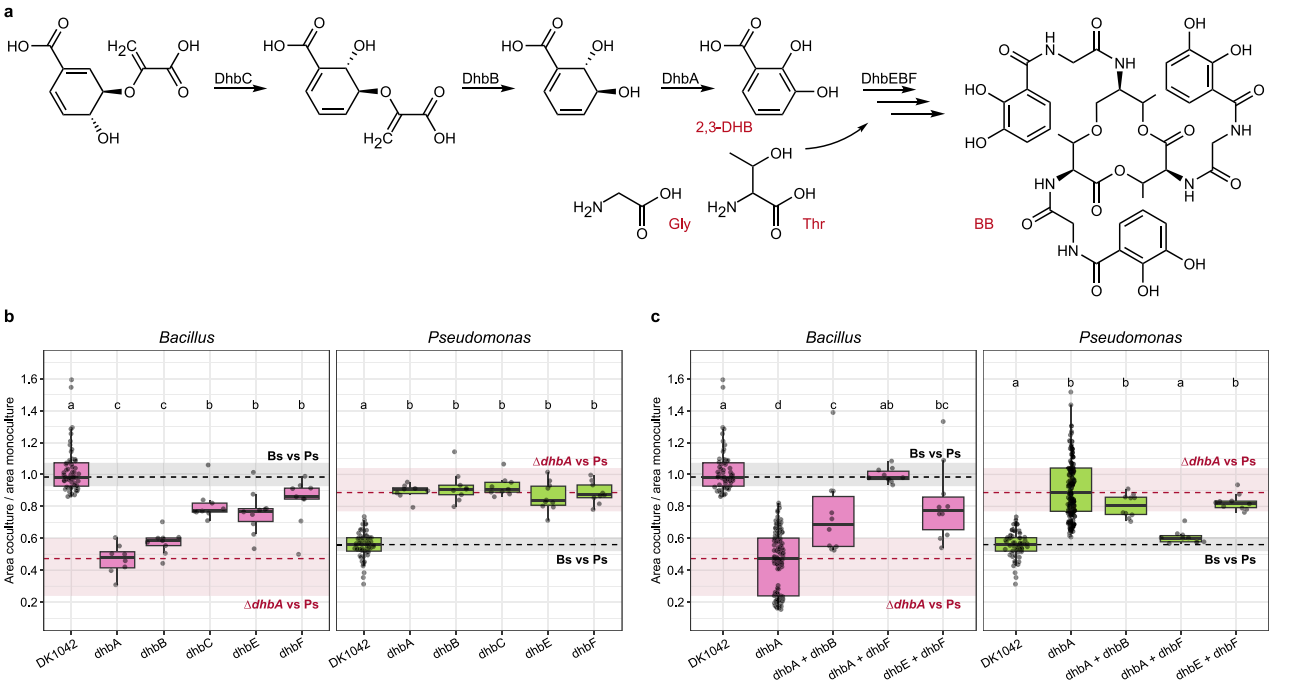

Figure 2. BB precursors are "public goods"; (A) BB is produced by the biosynthetic enzymes DhbACEBF from chorismate to 2,3-DHB, which is then used as a starting unit by the nonribosomal synthase complex DhbEBF to cyclize three monomers of 2,3-DHB using glycine (Gly) and threonine (Thr) linkers; (B) relative colony areas of PS92 and individual Δ*dhbA-F* gene deletion mutants; (C) relative colony areas of PS92 and combinations of Δ*dhbA-F* gene deletion mutants; black dashed lines and grey rectangles denote the mean relative colony size in the DK1042 + PS92 interaction (lines = mean, rectangles = min and max); red dashed lines and rectangles denote similarly for the Δ*dhbA* + PS92 interaction; grouping letters are from ANOVA with Tukey–Kramer's *post hoc* test; identical letters within each plot indicate a statistically significant grouping ($P < .05$, $n > 8$, from three independent experiments).

By measuring the areas of colonies, we determined that the growth of PS92 cocultured next to DK1042 was restricted, and after 72 h, the area of monoculture colonies was approximately twice that of the area of coculture colonies (Fig. 1B; Friedman one-way repeated measured ANOVA, $P = 1.67 \times 10^{-25}$, $n = 60$, df = 2). The Δ*dhbA* mutant did not surround nor restrict the growth of PS92 ($P = .321$, $n = 80$, df = 2), but rather was itself restricted ~2-fold ($P = 3.71 \times 10^{-28}$, $n = 80$, df = 2). The restriction in area is reflected in the number of colony-forming units from colonies in each interaction, showing a 16-fold reduction in cells in PS92 colonies grown next to DK1042 (Fig. 1C; Wilcoxon rank sum test, $P = 1.08 \times 10^{-5}$, $n = 20$, df = 18) and a 10^3-fold reduction in cells from Δ*dhbA*-mutant colonies grown next to PS92 ($P = 8.23 \times 10^{-5}$, $n = 17$, df = 15). When coculturing the strains in liquid medium, we observed inhibition of PS92 in KB broth regardless of whether the coculture was with DK1042 or Δ*dhbA*. Neither DK1042 nor Δ*dhbA* was antagonized by PS92, demonstrating that the observed antagonism is specific to solid media (Supplementary Fig. S1D and E). We also observed that the interaction occurs on LBGM but not on MSgg, and that glycerol is likely implicated in the antagonism (Supplementary Fig. S2).

In previous studies, BB production was reported to be linked to iron stress conditions [10]. As both LB and KB contain sources of natural iron from tryptone or yeast extract, low BB production could be expected on both types of media. LC–MS was used to compare BB production from DK1042 inoculated in liquid and solid LB and KB, revealing a 10-fold increase in BB concentration on solid KB compared to solid LB (Fig. 1D), while virtually undetectable in liquid media (Supplementary Fig. S3). The dependency on *dhbA* for antagonism and defence coupled with the exclusive production on solid KB suggests either a BB or DHB-mediated regulation in DK1042. However, a previous study showed that in *B. subtilis* biofilms, BB but not DHB is dispensable in air–liquid interface pellicle biofilms [9]. Thus, we tested whether BB or any precursor from the *dhbA-F* pathway influenced the pairwise interaction (Fig. 2A) and found all mutants unable to antagonize PS92 (Fig. 2B; one-way ANOVA with *post hoc* Tukey HSD, $P < 2.23 \times 10^{-10}$, $n > 10$, $df_w = 99$), suggesting that BB, and not an intermediate, must be present for antagonism.

Bacillibactin precursors are "public goods"

Since DHB has been shown to function as a siderophore in biofilms [7], we hypothesized that it could be used as a "public good" (here, a resource that can be produced by and shared among members of the population) and taken up by Δ*dhbA* mutant cells. Therefore, we mixed mutants disrupted in early biosynthesis (Δ*dhbA* and Δ*dhbB*), late biosynthesis (Δ*dhbE* and Δ*dhbF*), and mutants disrupted in both early and late biosynthesis (Δ*dhbA* and Δ*dhbF*) that should be able to complement each other through Δ*dhbF* supplying DHB to Δ*dhbA*, which then completes the synthesis of BB. Only the mixture of Δ*dhbA* and Δ*dhbF* was able to antagonize and restrict the growth of PS92 on solid KB medium (Fig. 2C; one-way ANOVA with *post hoc* Tukey HSD, $P = 5.92 \times 10^{-8}$, $n > 10$, $df_w = 207$), which not only demonstrates the ability of the mutants to complement each other, but also confirms that BB, and not DHB, is responsible for the antagonistic interaction between DK1042 and PS92. This was further corroborated by mixing DK1042 with Δ*dhbA* (unable to produce DHB) or Δ*dhbF* (unable to synthesize the nonribosomal peptide) using 1:1, 1:10, and 1:100 ratios, respectively, and spotted mixtures next to PS92 (Supplementary Fig. S4). Both mutants were rescued by the WT strain, even at a ratio of 1:100, and expansion of PS92 colonies was restricted independently of which mutant was used in the mixture or the ratio of the mixed strains.

Excess iron abolishes antagonism

Given that BB is the main siderophore of *B. subtilis*, we hypothesized that the antagonism was driven by iron in the media. To test this hypothesis, we cocultured DK1042 and PS92 on KB agar supplemented with varying concentrations of the ferrous iron chelator BPD (Fig. 3A) or with excess ferric iron either as ferric citrate, which is not transported into the cell via the BB and FeuABC-YusV machinery (Fig. 3B), or as $FeCl_3$ from which iron is readily bound to DHB and BB (Fig. 3C) [6, 9]. Curiously, sequestration of Fe(II) and addition of Fe(III) resulted in increased coculture colony size for the Δ*dhbA* mutant (one-way ANOVA resulted in nonsignificant differences between groups). Sequestering ferrous iron did not lead Δ*dhbA* to regain the ability to restrict PS92 size (one-way ANOVA with *post hoc* Tukey HSD, $n > 4$, df (residuals) = 29, $P < .03$), but, independently of concentration, both the addition of $FeCl_3$ and ferric citrate did (Fig. 3B and C), even though Δ*dhbA* should be unable to utilize $FeCl_3$ [49]. Similarly, the Δ*besA* mutant, unable to release iron from BB, was also complemented by any iron-related change to the medium. However, the Δ*feuA* mutant did not respond to $FeCl_3$ (as expected) but could be complemented by ferric citrate in a dose-dependent manner.

DK1042 heavily alters the PS92 transcriptome

To better understand the transcriptional landscape present in each strain as a result of cocultivation, we extracted total RNA from colonies cultured in monoculture or with an interaction partner ($n = 3$ for all samples). This allowed us to identify transcriptional differences between DK1042 and Δ*dhbA* both in monoculture and coculture, but also between each individual strain in monoculture compared to coculture to ascertain how a neighbouring partner alters the transcription of a focal strain (Supplementary Fig. S5). Transcriptomic analysis revealed that the PS92 transcriptome was heavily altered by DK1042 (1036 differentially regulated genes at $\log_2(FC) > |2|$ and adjusted $P < .01$) but not by Δ*dhbA* (9 differentially regulated genes). Approximately, 4%–8% of the transcriptomes of DK1042 and Δ*dhbA* (364 and 172 differentially regulated genes, respectively) were differentially regulated by the presence of PS92, but comparison of cocultures revealed that 1002 transcripts were differentially regulated between the two strains in coculture. In monoculture, 395 transcripts were differentially regulated between DK1042 and Δ*dhbA*.

Δ*dhbA* downregulates sporulation and biofilm formation

When coculturing DK1042 with PS92, genes related to sporulation and germination were upregulated in DK1042 (Fig. 4A), though not differentially regulated in the Δ*dhbA* mutant in coculture compared with its monoculture. However, comparing the levels of transcription between DK1042 and Δ*dhbA* reveals that lack of *dhbA* strongly downregulated sporulation and germination pathways, independently of whether it was cocultured with PS92.

Elimination of DHB and BB production affected several genes related to biofilm formation and sporulation in the *epsA-O*, *tapA-tasA-sipW*, *spsA-L*, *cot* and *spoII*, *III*, *IV*, *V*, and *VI* operons, an effect reported previously [9, 49]. In addition, the transcription level of the *sinI* gene was higher in monoculture for Δ*dhbA* compared with DK1042, though not in coculture. In coculture, the lack of *dhbA* upregulated the transcription of the biofilm repressor gene *abrB*.

Repression of sporulation and biofilm formation was further corroborated by the downregulation of genes involved in utilization of glutamine, manganese, and glycerol. Manganese and glutamine/glutamate utilizations are well known for their role in the Spo0A sporulation pathway that drives both biofilm formation and sporulation [50-53], while manganese homeostasis was very recently shown to be tightly interlinked with iron homeostasis [54].

The transcriptome of the Δ*dhbA* mutant did not display signs of iron starvation, with the exception of a slight repression in the transcription of *fur* when comparing transcription of monocultures. The *dhb*, *feu*, *yusV*, *besA*, and *yvm* genes were not differentially regulated in the Δ*dhbA* mutant compared with DK1042, except the *dhbA* transcript level, which was deleted in the genome of the mutant and therefore transcriptionally absent in the mutant. Additionally, genes involved in production of known bioactive secondary metabolites were not differentially regulated in *Bacillus* regardless of the mutation or coculture partner.

PS92 downregulates Gac/Rsm and iron acquisition in coculture with DK1042

When cocultured with DK1042, PS92 underwent downregulation of biosynthetic genes responsible for production of several secondary metabolites (Fig. 4B and Supplementary Dataset S1). All biosynthetic genes involved in Pvd, alginate (Alg), and viscosin production were repressed along with a Type VI secretion system (T6SS) subtype i3, while genes responsible for Type II and III secretion and reactive oxygen neutralization were upregulated. Similar changes have previously been observed in the closely related *P. fluorescence* SBW25 when removing the histidine kinase *gacS* (OrthoANIu similarity between SBW25 and PS92 = 99.06%) [55]. The Gac/Rsm pathway is a conserved two-component system found in many γ-proteobacteria and known to positively regulate biofilm formation and secondary metabolism in most pseudomonads and induce virulence factors in plant pathogenic species. Indeed, PS92 *gacS* (FNPKGJ_17835) was downregulated 4-fold in PS92 when cocultured with DK1042 but not when cocultured with Δ*dhbA*.

Although Pvd biosynthetic genes were downregulated, the iron starvation sigma factor-encoding gene *pvdS* (FPNKGJ_22055) had a higher transcript level in coculture with DK1042. Pvd is the primary siderophore in SBW25 [56], though other iron-chelating molecules are encoded in the genomes of both SBW25 [55] and PS92. A biosynthetic gene cluster encoding the production machinery for a corrugatin-like molecule (FNPKGJ_15100–15175) was similarly repressed ($P.adj < .05$), although not below the threshold of $\log_2(FC) < -2$.

We found further evidence for the repression of the Gac/Rsm system in mass spectrometry imaging of cocultures, which showed that several molecules produced by genes under the control of the Gac/Rsm system were absent from cocultures with DK1042 but present in monoculture colonies and cocultures with Δ*dhbA* (Fig. 4C). The presence of viscosin in all cultures except coculture with DK1042 on KB prompted us to test if viscosin was the antagonistic molecule against Δ*dhbA*. In lieu of a PS92 Δ*viscA* gene deletion mutant, we obtained a *Pseudomonas fluorescens* SBW25 Δ*viscA* mutant with an identical interaction with DK1042, but found that Δ*viscA* was still able to antagonize Δ*dhbA*, similarly to the WT strain (Supplementary Fig. S6).

Antagonism depends on bacillibactin

Based on the transcriptome data for DK1042, we screened multiple gene disruption mutants for their antagonistic effect against PS92 (Fig. 5). Effects of mutations ranged from deficiency in the production of biofilm matrix (*epsA-O*, *tasA*) and secondary metabolites (*srfAA*, *pksL*, *sfp*, *cypX*, *yvmC*) to lacking sensor kinases (*kinA-E*) or being unable to undergo sporulation (*spo0A*). Only

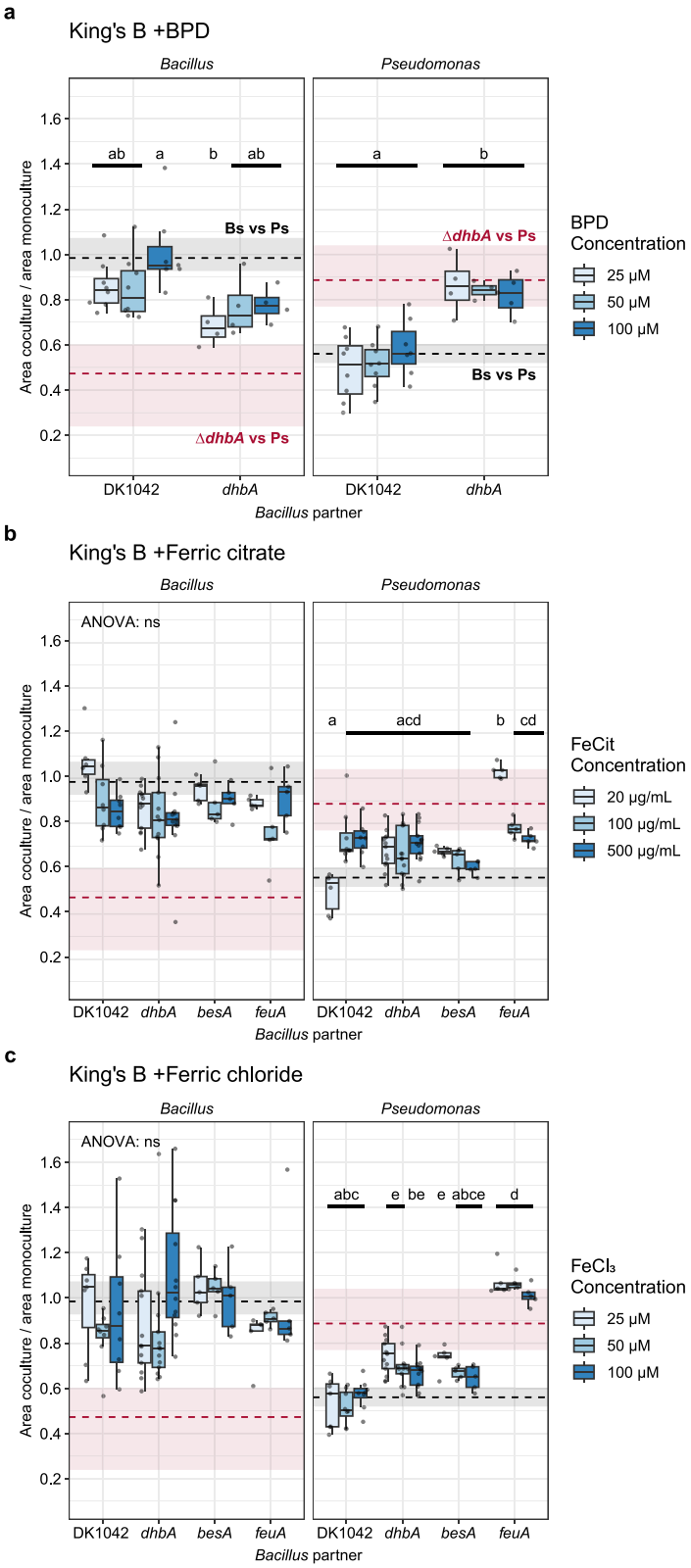

Figure 3. Excess iron restores mutant bacilli offensive and defensive attributes; *Bacillus* and *Pseudomonas* relative colony areas on KB with increasing concentrations of (A) Fe(II) chelator 2,2- BPD, (B) ferric citrate (FeCit), and (C) ferric chloride ($FeCl_3$); PS92 was spotted next to DK1042 or mutants deficient in the BB biosynthesis and uptake pathway; dashed lines and rectangles are median, first and third quartiles for PS92 colonies spotted next to Δ*dhbA* (above) and DK1042 (below) on nonsupplemented KB; grouping letters are from ANOVA with Tukey–Kramer's *post hoc* test; identical letters within each plot indicate a statistically significant grouping ($P < .05$, $n \geq 4$ colonies from two independent experiments).

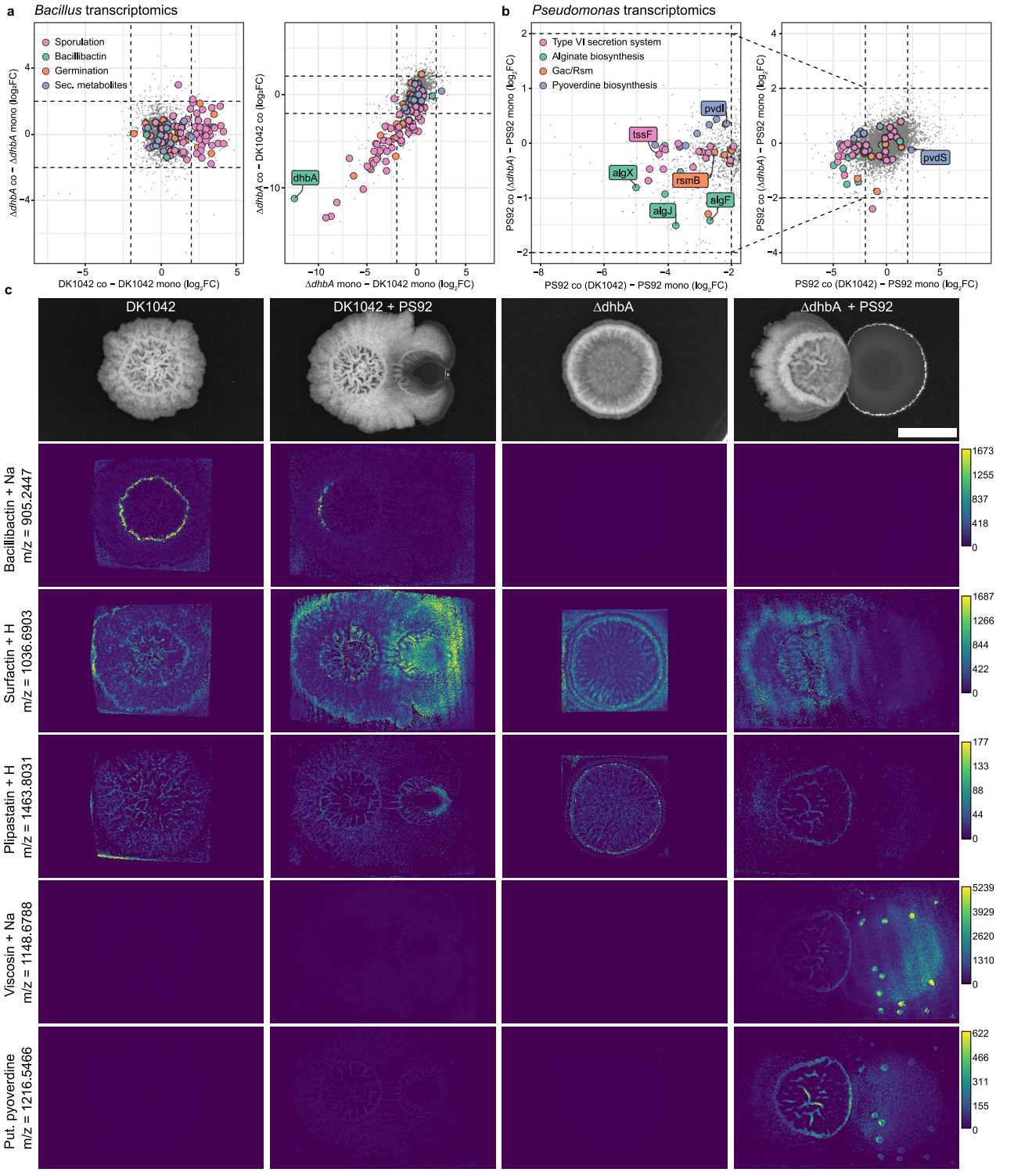

Figure 4. DK1042 alters PS92 transcriptome and metabolome via *gac*S; (A) Δ*dhbA* downregulates genes related to sporulation and germination independently of having PS92 as its interaction partner; DK1042-upregulated genes of the same category only when in coculture with PS92; dashed lines indicate log2(FC) = |2|; (B) several biosynthetic pathways related to the Gac/Rsm two-component system were significantly downregulated ($\log_2(FC) < -2$ and adjusted *P*-value < .01) in coculture with DK1042, except for the alternative sigma factor *pvd*S; (C) mass spectrometry imaging reveals the presence/absence of select metabolites as well as their spatial localization in the interactions; scale bar = 5 mm; grey values are root mean squared intensity across all samples, and lookup tables were scaled identically across each metabolite; NaN pixels were set to zero; metabolites were annotated with metaspace using the 2019 Natural Product Atlas database; m/z = 1216.5466 was manually annotated as a Pvd structure.

three mutants were significantly unable to antagonize PS92 (one-way ANOVA with *post hoc* Tukey HSD, $n = 4$, $df_w = 212$; Δ*sfp*-DK1042 $P = 1.32 \times 10^{-6}$, Δ*feuA*-DK1042 $P = 1.29 \times 10^{-5}$, and Δ*glpK*-DK1042 $P = .019$). Thus, neither sporulation nor biofilm formation are essential for antagonism, and likewise, typical secondary metabolites with antimicrobial properties such as surfactin and bacillaene had no effect on the restriction of PS92 colony area (although this was suggested from the mass spectrometry

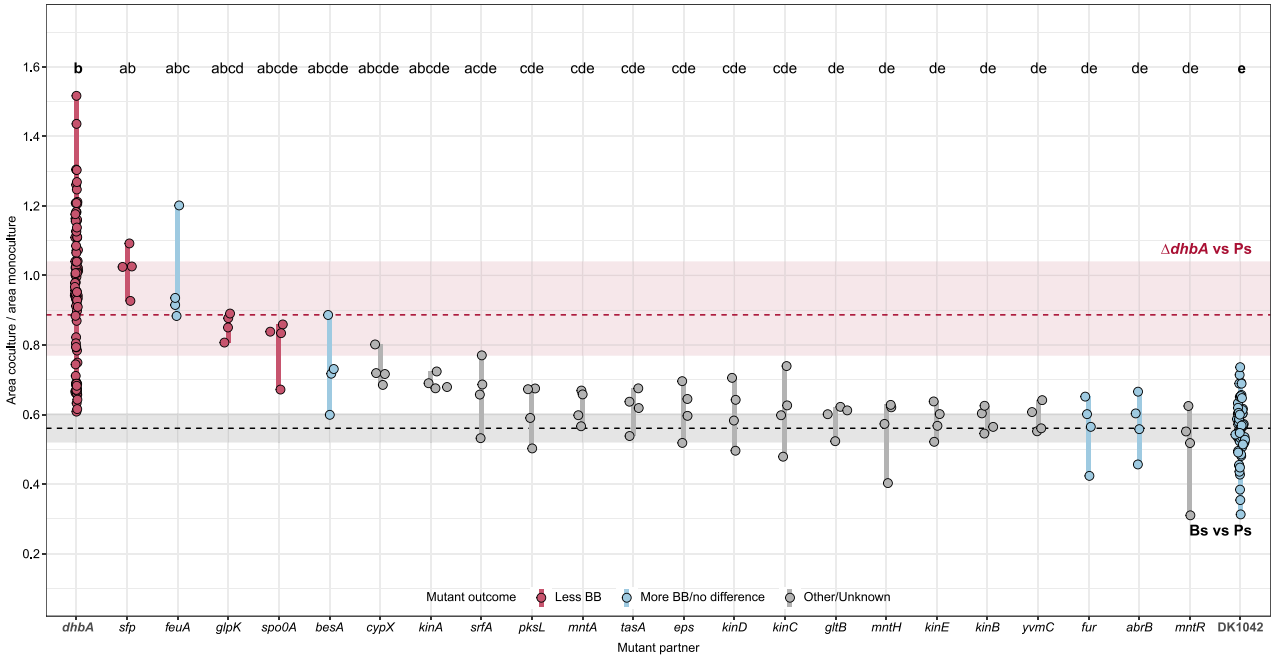

Figure 5. *Pseudomonas* colony size restriction is related to *sfp* and *feuA*: PS92 colony size was measured in cocultures next to Bacillus gene deletion mutants deficient in multiple aspects of cell physiology; colonies spotted next to mutants lacking sfp, feuA, and glpK were significantly larger than those spotted next to DK1042 relative to monoculture colony size, while not being significantly smaller than colonies spotted next to ΔdhbA; other mutants related to biofilm formation, metal homeostasis, and bioactive secondary metabolites were not diminished in their restriction of PS92; dashed lines and rectangles are median, first and third quartiles for PS92 colonies spotted next to ΔdhbA and DK1042; grouping letters are from ANOVA with Tukey–Kramer's *post hoc* test; identical letters within each plot indicate a statistically significant grouping ($P < .05$, $n = 4$ biologically independent colonies). dhbA and DK1042 represent pooled data from multiple experiments ($n > 80$).

imaging). The inability of Δ*feuA* to antagonize suggests that iron uptake by BB is essential for restriction of PS92 colony size, but the fitness of the Δ*feuA* mutant was rather low even in monoculture (Supplementary Fig. S7), which could result in low metabolic output in general.

Interaction is conserved across fluorescent *Pseudomonas* isolates

To determine if the iron-related antagonism is specific to DK1042 and PS92, we cocultured DK1042 and Δ*dhbA* on KB agar with a collection of 16 fluorescent *Pseudomonas* soil isolates for which genomes had been sequenced (Fig. 6). Thus, we could qualitatively compare the interaction outcome with the genomic presence of biosynthetic pathways. Multiple isolates were restricted in colony size by DK1042 and not by Δ*dhbA*. Most isolates also seemed to influence the size and/or morphology of Δ*dhbA*, except XL272 (previously *Pseudomonas stutzeri*, now *Stutzerimonas degradans*), which is the only isolate lacking the Gac/Rsm-controlled biosynthetic machineries producing Pvd and Alg. A few isolates belonging to *Pseudomonas corrugata* and *protegens* subgroups were able to inhibit both DK1042 and Δ*dhbA*, which may be attributed to their potential for producing 2,4-diacetylphloroglucinol and pyoluteorin [57]. Strains from other *P. fluorescens* subgroups were all restricted in colony growth in the presence of BB-producing *B. subtilis*, demonstrating the conservation of this antagonism across species.

Discussion

In this study, we report a novel siderophore-mediated antagonism conserved between *B. subtilis* and multiple *Pseudomonas* spp. We show that the interaction is dependent on iron and BB, and that a lack of BB on KB agar results in both diminished offence and defence. The consequence of BB-mediated antagonism is a restriction of *Pseudomonas* colony spreading and a reduction both in transcription and production of several products related to the secondary metabolism-regulating Gac/Rsm system, which over time allows *Bacillus* to overgrow a *Pseudomonas* colony.

Our results show a strong implication of BB in the antagonism between DK1042 and PS92. Disrupting individual iron homeostasis-related genes diminished their antagonistic properties, and coculturing mutants in mixed cultures restored their properties. This indicates that the critical components of the DhbA-F pathway can be secreted and shared between members in a population as "public goods."

Bacillus colony expansion in coculture is especially affected by iron availability (Fig. 3). Though the iron concentration added to the medium in these experiments was relatively high, the results suggest that the interaction, both defensive and offensive, is iron-dependent. Iron homeostasis, biofilm formation, and sporulation are tightly interlinked in *B. subtilis*, and DhbA is essential for structured biofilm formation and proper sporulation due to the high iron demands of these lifestyles [9, 49, 58]. In our coculture assays, lack of *dhbA* negatively affected multiple biofilm-related genes repressing biofilm formation and sporulation. This suggests that the Δ*dhbA* mutant did not form a biofilm or undergo sporulation either in coculture or in monoculture. The production of a matrix and the formation of spores as defensive measures in microbial ecology have received little attention [59] despite investigations into their relation to T6SS [24, 60]. Defence appears to take precedence for *Bacillus* in the present antagonism, and a biofilm- and sporulation-deficient mutant may be too antagonized by PS92 to produce the necessary effector for growth restriction. This could explain our observations with Δ*feuA* which requires large quantities of supplemented iron for growing comparably to the wild type (Fig. 3B and C). Additionally, a biofilm-proficient strain

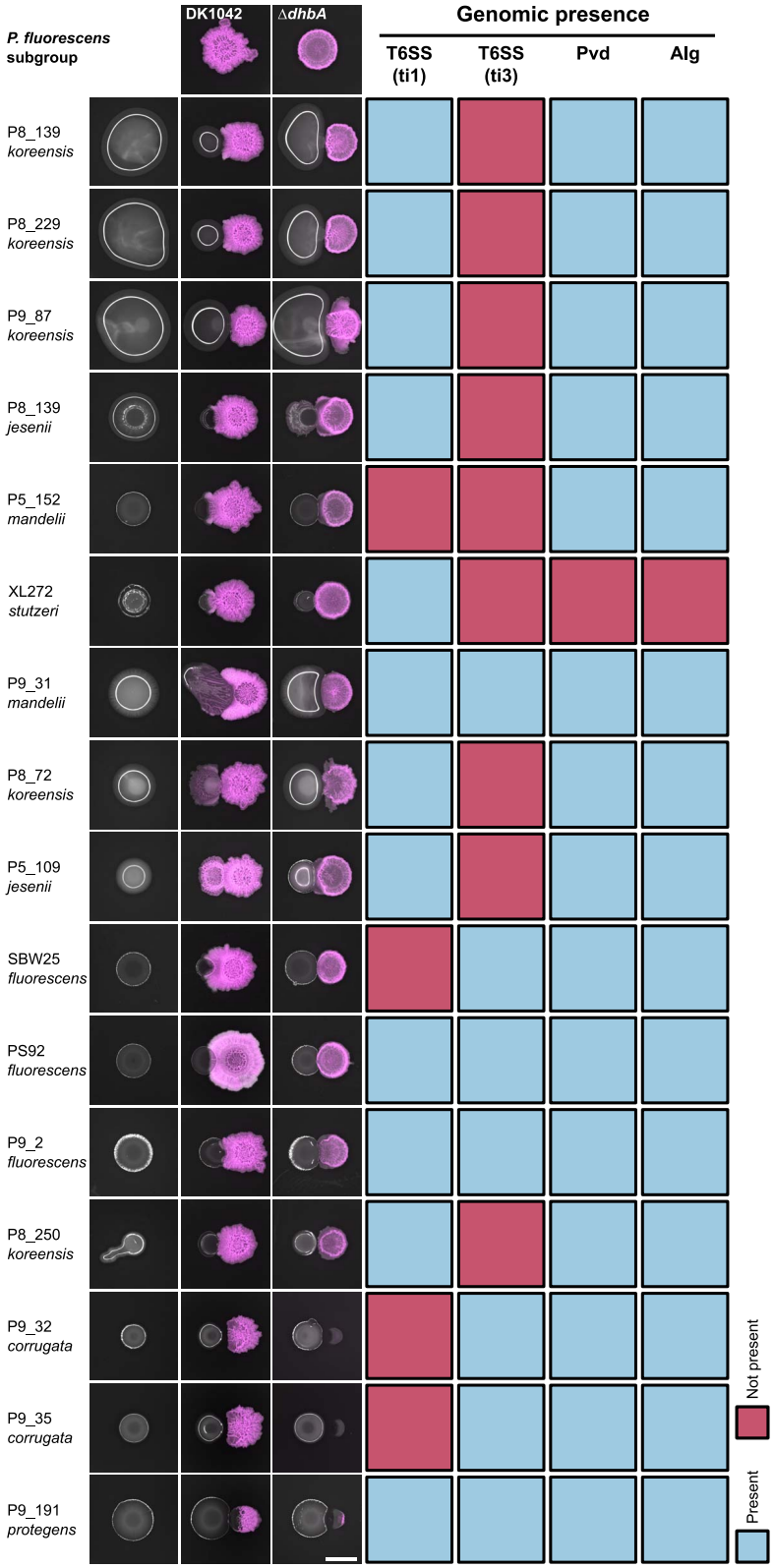

Figure 6. Antagonism is conserved across *Pseudomonas* spp.; fluorescent *Pseudomonas* soil isolates were cultured next to DK1042 or Δ*dhbA* on KB agar and their genomes were assessed for the presence of Gac-/Rsm-related biosynthetic genes; presence of >80% of PS92 genes at 40% amino acid identity was scored as "present" (blue boxes), while any less was scored as "not present" (red boxes); isolates are presented as their strain ID and the closest related *P. fluorescens* subgroup as described by Hesse *et al.* based on whole-genome alignments; T6SS, Type VI secretion system; ti1, Type i1; ti3, Type i3.

lacking the antagonistic molecule may block PS92 growth through spatial competition [61-63], though it will be unable to restrict colony spreading chemically. Another possibility could be that BB is a stronger iron chelator than Pvd, sequestering Fe(III) away from *Pseudomonas* and thereby inducing iron starvation. When *Bacillus* is unable to produce BB, the tide turns, and Pvd from

Pseudomonas sequesters Fe(III) away from *Bacillus*. Pvd production on KB has been shown in several pseudomonads to be negatively correlated with iron content, where the iron-binding Fur represses Pvd production through repression of *pvdS* [56]. This could explain how Δ*dhbA*, Δ*besA*, and Δ*feuA* are rescued by iron supplementation even in the form of ferric chloride (Fig. 3B). When iron is present, Pvd is not produced, and the *Bacillus* iron homeostasis mutants are not inhibited by iron competition. With this mechanism, strong iron starvation responses are likely in both *Bacillus* and *Pseudomonas*, but in Δ*dhbA*, iron homeostasis was not significantly upregulated in coculture with PS92 (Fig. 4A). On the other hand, *pvdS* in PS92 was significantly upregulated (Fig. 4B), which is indicative of iron starvation, but without the complementary upregulation of the rest of the Pvd biosynthetic genes. Thus, it is unclear whether the consequence of coculture is iron starvation, repression of the Gac/Rsm pathway, or a combination of both.

In *P. aeruginosa*, Gac/Rsm is known to positively regulate Pvd biosynthetic gene transcription trough PvdS [64, 65], and a similar phenotype has been described in *P. fluorescens* SBW25 [55]. Recently, both Pvd and, to a larger extent, pyochelin were shown to be sensed by *Bacillus velezensis*, instigating mobilization of secondary metabolites [21]. Although sensing of pyochelin occurs independently of iron and BB, Pvd was shown to increase the production of BB. PS92 does not contain a gene cluster encoding the synthetic machinery for any type of pyochelin, and thus, pyochelin sensing presumably does not occur in the interaction between DK1042 and PS92.

Our results suggest a *Bacillus*-mediated repression of *gacS*, a phenomenon with precedent from interaction between a *Bacillus* sp. isolate and *P. syringae* pv. Tomato DC3000 [66]. However, neither previous nor our experiments reveal if *gacS* repression is directly caused by DK1042 or by a sensory mechanism in PS92. Currently, there is no consensus on exactly which ligand triggers the Gac signal cascade [67], although it is expected that secreted products resulting from the activated pathway itself are at least partly responsible [68]. However, in *Pseudomonas*, GacS is activated and inhibited by the transmembrane receptors LadS and RetS, respectively, which in turn are activated by calcium ions (LadS) and mucin glycans or temperature (RetS) [69-71]. It is also hypothesized that the Gac/Rsm pathway functions via an alternative quorum sensing pathway, and that induction is achieved at higher cell densities [68]. This might explain why *gacS* was downregulated in PS92 spotted next to DK1042, where the colony is indeed restricted in size and at a lower cell density. Large-scale purification and chemical synthesis of BB were unsuccessful in our study; hence, we could not directly probe the antagonistic properties of BB. Siderophores have long been implicated in microbial interactions, particularly in iron-scarce environments. In infections, Pvd and enterobactin are essential for *P. aeruginosa* and *E. coli*, respectively, not only due to iron requirements in a complex environment, but also in polymicrobial interactions as interspecies competitive factors [72]. Siderophores are also thought to play a role in the biocontrol of plant pathogens by both *Pseudomonas* and *Bacillus*, but a thorough examination of the literature reveals that *Bacillus* and *Pseudomonas* siderophores have only rarely been directly implicated in interspecies interactions *in planta* [13]. Most evidence originated in the previous millennium where *Pseudomonas* siderophores proved to be determinants of microbial interactions through iron sequestration [73, 74]. Others have since inferred biocontrol potential from the ability to produce siderophores without experimentally determining the consequence of losing siderophore production [10, 75]. Our study systematically investigated the significance of BB and its effects on transcription and metabolite production in microbial interactions. Although we demonstrated the importance of BB on rich media, our study complements and expands the previously established role of BB in biocontrol. We found that *Bacillus* inhibition of colony expansion could be replicated qualitatively with multiple fluorescent *Pseudomonas* spp., and that disrupting *dhbA* abolished the antagonism (Fig. 6). The generality of this interaction against multiple pseudomonads is intriguing, in the potential for *B. subtilis* to compete against *Pseudomonas* spp. in soil. Although our *P. marginalis* isolate proved nonpathogenic against lettuce, cabbage, and spinach, many pseudomonads are pathogenic and could potentially be controlled by *Bacillus* producing BB. As BB production is conserved across many species of *Bacillus*, one would expect that other bacilli would display similar BB-dependent antagonism against *Pseudomonas*, though this remains to be experimentally validated. The lack of PS92 plant colonization meant that we were unable to determine if BB-mediated antagonism occurs in the phyllosphere as well as on agar surfaces. The medium specificity of this interaction is not surprising, as pairwise interactions have been found to always be context dependent [76]. We observed glycerol to possess some role in the antagonism, but only on solid medium (Supplementary Fig. S2). It is unclear why the antagonism was not present in the same form in liquid media (Supplementary Fig. S1D and E). Other studies have successfully transferred biocontrol properties from *in vitro* to *in planta* [77], but the medium dependency of the antagonism between DK1042 and PS92 might render it difficult to apply to agriculture. Regardless, understanding the molecular mechanism underlying the antagonism could allow the environment to be tailored specifically to the intended interaction. Future studies should investigate the apparent iron competition between BB and Pvd, as well as the hypothesis that BB represses Gac sensing in fluorescent pseudomonads.

Acknowledgements

The authors thank Lars Jelsbak and Morten Lindquist Hansen for contributing *Pseudomonas* soil isolates for this study, and the DTU Metabolomics Core for MSI and LC–MS instrumentation.

Author contributions

Mark Lyng and Ákos T. Kovács designed the study; Mark Lyng, Johan P.B. Jørgensen, and Scott A. Jarmusch collected and analysed data; Morten D. Schostag, Diana K.C. Aguilar, and Carlos N. Lozano-Andrade contributed with methodology or preliminary data; Mark Lyng and Ákos T. Kovács wrote first draft of paper with edits from all authors.

Supplementary material

Supplementary material is available at *The ISME Journal* online.

Conflicts of interest

None declared.

Funding

This project was funded by a DTU Alliance Strategic Partnership PhD fellowship, by the Danish National Research Foundation (DNRF137) for the Center for Microbial Secondary Metabolites, and the Novo Nordisk Foundation within the INTERACT project

of the Collaborative Crop Resiliency Program (NNF19SA0059360) and for the "Imaging microbial language in biocontrol (IMLiB)" infrastructure grant (NNF19OC0055625).

Data availability

Analysis scripts and processed data have been deposited at Github. (https://github.com/marklyng/dhb_repository). Genome assemblies have been deposited at NCBI (accession numbers are listed in Table S1). Raw sequence reads (long- and short-gDNA reads and RNA) have been deposited at the Sequencing Read Archive (SRA; https://www.ncbi.nlm.nih.gov/sra) with BioProject ID PRJNA956831. Raw microscopy images have been deposited at Dryad (https://datadryad.org/; DOI https://doi.org/10.5061/dryad.vq83bk3zc). MSI data have been deposited at Metaspace [78] under project ID. https://metaspace2020.eu/project/lyng-2023. LC–MS data have been deposited at GNPS-MassIVE under MSV000092142.

References

1. Andrews SC, Robinson AK, Rodríguez-Quiñones F. Bacterial iron homeostasis. *FEMS Microbiol Rev* 2003;**27**:215–37.
2. Kramer J, Özkaya Ö, Kümmerli R. Bacterial siderophores in community and host interactions. *Nat Rev Microbiol* 2020;**18**:152–63.
3. Rehm K, Vollenweider V, Gu S *et al.* Chryseochelins—structural characterization of novel citrate-based siderophores produced by plant protecting *Chryseobacterium* spp. *Metallomics* 2023;**15**:mfad008.
4. Dertz EA, Stintzi A, Raymond KN. Siderophore-mediated iron transport in *Bacillus subtilis* and *Corynebacterium glutamicum*. *J Biol Inorg Chem* 2006;**11**:1087–97.
5. Miethke M, Schmidt S, Marahiel MA. The major facilitator superfamily-type transporter YmfE and the multidrug-efflux activator Mta mediate bacillibactin secretion in *Bacillus subtilis*. *J Bacteriol* 2008;**190**:5143–52.
6. Ollinger J, Song KB, Antelmann H *et al.* Role of the fur regulon in iron transport in *Bacillus subtilis*. *J Bacteriol* 2006;**188**:3664–73.
7. Miethke M, Klotz O, Linne U *et al.* Ferri-bacillibactin uptake and hydrolysis in *Bacillus subtilis*. *Mol Microbiol* 2006;**61**:1413–27.
8. May JJ, Wendrich TM, Marahiel MA. The *dhb* operon of *Bacillus subtilis* encodes the biosynthetic template for the catecholic siderophore 2,3-dihydroxybenzoate-glycine-threonine trimeric ester bacillibactin. *J Biol Chem* 2001;**276**:7209–17.
9. Qin Y, He Y, She Q *et al.* Heterogeneity in respiratory electron transfer and adaptive iron utilization in a bacterial biofilm. *Nat Commun* 2019;**10**:3702.
10. Dimopoulou A, Theologidis I, Benaki D *et al.* Direct antibiotic activity of bacillibactin broadens the biocontrol range of *Bacillus amyloliquefaciens* MBI600. *mSphere* 2021;**6**:e00376–21.
11. Chakraborty K, Kizhakkekalam VK, Joy M *et al.* Bacillibactin class of siderophore antibiotics from a marine symbiotic *Bacillus* as promising antibacterial agents. *Appl Microbiol Biotechnol* 2022;**106**:329–40.
12. Nalli Y, Singh S, Gajjar A *et al.* Bacillibactin class siderophores produced by the endophyte *Bacillus subtilis* NPROOT3 as antimycobacterial agents. *Lett Appl Microbiol* 2022;**76**:ovac026.
13. Lyng M, Kovács ÁT. Frenemies of the soil: *Bacillus* and *Pseudomonas* interspecies interactions. *Trends Microbiol* 2023;**31**:845–57.
14. Gross H, Loper JE. Genomics of secondary metabolite production by *Pseudomonas* spp. *Nat Prod Rep* 2009;**26**:1408–46.
15. Kaspar F, Neubauer P, Gimpel M. Bioactive secondary metabolites from *Bacillus subtilis*: a comprehensive review. *J Nat Prod* 2019;**82**:2038–53.
16. Cesa-Luna C, Geudens N, Girard L *et al.* Charting the lipopeptidome of nonpathogenic *Pseudomonas*. *mSystems* 2023;**8**:e00988–22.
17. Sun X, Xu Z, Xie J *et al.* *Bacillus velezensis* stimulates resident rhizosphere *Pseudomonas stutzeri* for plant health through metabolic interactions. *ISME J* 2022;**16**:774–87.
18. Liu Y, Xu Z, Xun W *et al.* Plant beneficial bacterium promotes plant growth by altering social networks of bacteria in the rhizosphere. *Res Sq* 2023; preprint. https://doi.org/10.21203/rs.3.rs-2491444/v1.
19. Trivedi P, Leach JE, Tringe SG *et al.* Plant–microbiome interactions: from community assembly to plant health. *Nat Rev Microbiol* 2020;**18**:607–21.
20. Wei Z, Gu Y, Friman V-P *et al.* Initial soil microbiome composition and functioning predetermine future plant health. *Sci Adv* 2019;**5**:eaaw075.
21. Andrić S, Rigolet A, Argüelles Arias A *et al.* Plant-associated *bacillus* mobilizes its secondary metabolites upon perception of the siderophore pyochelin produced by a *Pseudomonas* competitor. *ISME J* 2023;**17**:263–75.
22. Andrić S, Meyer T, Rigolet A *et al.* Lipopeptide interplay mediates molecular interactions between soil *Bacilli* and *Pseudomonads*. *Microbiol Spectr* 2021;**9**:e02038–21.
23. Molina-Santiago C, Vela-Corcía D, Petras D *et al.* Chemical interplay and complementary adaptative strategies toggle bacterial antagonism and co-existence. *Cell Rep* 2021;**36**:109449.
24. Molina-Santiago C, Pearson JR, Navarro Y *et al.* The extracellular matrix protects *Bacillus subtilis* colonies from *Pseudomonas* invasion and modulates plant co-colonization. *Nat Commun* 2019;**10**:1919.
25. Pérez-Lorente AI, Molina-Santiago C, de Vicente A *et al.* Sporulation activated via σ^W protects *Bacillus* from a Tse1 peptidoglycan hydrolase type VI secretion system effector. *Microbiol Spectr* 2023;**11**:e05045–22.
26. Charron-Lamoureux V, Haroune L, Pomerleau M *et al.* Pulcherriminic acid modulates iron availability and protects against oxidative stress during microbial interactions. *Nat Commun* 2023;**14**:2536.
27. Schindelin J, Arganda-Carreras I, Frise E *et al.* Fiji: an open-source platform for biological-image analysis. *Nat Methods* 2012;**9**:676–82.
28. Otsu N. A Threshold Selection Method from Gray-Level Histograms, IEEE, 1979;**9**:62–66.
29. Koo BM, Kritikos G, Farelli JD *et al.* Construction and analysis of two genome-scale deletion libraries for *Bacillus subtilis*. *Cell Syst* 2017;**4**:291–305.e7.
30. Zobel S, Benedetti I, Eisenbach L *et al.* Tn7-based device for calibrated heterologous gene expression in *Pseudomonas putida*. *ACS Synth Biol* 2015;**4**:1341–51.
31. Kiesewalter HT, Lozano-Andrade CN, Wibowo M *et al.* Genomic and chemical diversity of *Bacillus subtilis* secondary metabolites against plant pathogenic fungi. *mSystems* 2021;**6**:e00770–20.
32. Wick RR, Judd LM, Cerdeira LT *et al.* Trycycler: consensus long-read assemblies for bacterial genomes. *Genome Biol* 2021;**22**:266.
33. Wick RR, Judd LM, Gorrie CL *et al.* Unicycler: resolving bacterial genome assemblies from short and long sequencing reads. *PLoS Comput Biol* 2017;**13**:e1005595.
34. Parks DH, Imelfort M, Skennerton CT *et al.* CheckM: assessing the quality of microbial genomes recovered from isolates, single cells, and metagenomes. *Genome Res* 2015;**25**:1043–55.
35. Alanjary M, Steinke K, Ziemert N. AutoMLST: an automated web server for generating multi-locus species trees highlighting natural product potential. *Nucleic Acids Res* 2019;**47**:W276–82.

36. Meier-Kolthoff JP, Göker M. TYGS is an automated high-throughput platform for state-of-the-art genome-based taxonomy. *Nat Commun* 2019;**10**:2182.
37. Schwengers O, Jelonek L, Dieckmann MA *et al.* Bakta: rapid and standardized annotation of bacterial genomes via alignment-free sequence identification. *Microb Genom* 2021;**7**: 000685.
38. Tonkin-Hill G, MacAlasdair N, Ruis C *et al.* Producing polished prokaryotic pangenomes with the Panaroo pipeline. *Genome Biol* 2020;**21**:180.
39. Bray NL, Pimentel H, Melsted P *et al.* Near-optimal probabilistic RNA-seq quantification. *Nat Biotechnol* 2016;**34**:525–7.
40. Pertea M, Pertea G. GFF utilities: GffRead and GffCompare. *F1000Res* 2020;**9**:304.
41. Love MI, Huber W, Anders S. Moderated estimation of fold change and dispersion for RNA-seq data with DESeq2. *Genome Biol* 2014;**15**:550.
42. RStudio Team. *RStudio: Integrated Development for R*. Boston, MA, 2019 (https://www.r-project.org).
43. R Core Team. *R: A Language And Environment For Statistical Computing*. Vienna, Austria, 2021 (https://www.R-project.org).
44. Wickham H, Averick M, Bryan J *et al.* Welcome to the Tidyverse. *J Open Source Softw* 2019;**4**:1686.
45. Cantalapiedra CP, Hernández Plaza A, Letunic I *et al.* eggNOG-mapper v2: functional annotation, orthology assignments, and domain prediction at the metagenomic scale. *Mol Biol Evol* 2021;**38**:5825–9.
46. Kanehisa M, Sato Y, Kawashima M. KEGG mapping tools for uncovering hidden features in biological data. *Protein Sci* 2022;**31**: 47–53.
47. Pedreira T, Elfmann C, Stülke J. The current state of *Subti*Wiki, the database for the model organism *Bacillus subtilis*. *Nucleic Acids Res* 2022;**50**:D875–82.
48. Winsor GL, Griffiths EJ, Lo R *et al.* Enhanced annotations and features for comparing thousands of *Pseudomonas* genomes in the *Pseudomonas* genome database. *Nucleic Acids Res* 2016;**44**:D646–53.
49. Rizzi A, Roy S, Bellenger J-P *et al.* Iron homeostasis in *Bacillus subtilis* requires siderophore production and biofilm formation. *Appl Environ Microbiol* 2019;**85**:e02439–18.
50. Mhatre E, Troszok A, Gallegos-Monterrosa R *et al.* The impact of manganese on biofilm development of *Bacillus subtilis*. *Microbiology* 2016;**162**:1468–78.
51. Shemesh M, Chaia Y. A combination of glycerol and manganese promotes biofilm formation in *Bacillus subtilis* via histidine kinase KinD signaling. *J Bacteriol* 2013;**195**:2747–54.
52. Kimura T, Kobayashi K. Role of glutamate synthase in biofilm formation by *Bacillus subtilis*. *J Bacteriol* 2020;**202**:00120–0.
53. Hassanov T, Karunker I, Steinberg N *et al.* Novel antibiofilm chemotherapies target nitrogen from glutamate and glutamine. *Sci Rep* 2018;**8**:7097.
54. Steingard CH, Pinochet-Barros A, Wendel BM *et al.* Iron homeostasis in *Bacillus subtilis* relies on three differentially expressed efflux systems. *Microbiology* 2023;**169**:001289.
55. Cheng X, de Bruijn I, van der Voort M *et al.* The Gac regulon of *Pseudomonas fluorescens* SBW25. *Environ Microbiol Rep* 2013;**5**: 608–19.
56. Moon CD, Zhang XX, Matthijs S *et al.* Genomic, genetic and structural analysis of pyoverdine-mediated iron acquisition in the plant growth-promoting bacterium *Pseudomonas fluorescens* SBW25. *BMC Microbiol* 2008;**8**:7.
57. Powers MJ, Sanabria-Valentín E, Bowers AA *et al.* Inhibition of cell differentiation in *Bacillus subtilis* by *Pseudomonas protegens*. *J Bacteriol* 2015;**197**:2129–38.
58. Pelchovich G, Omer-Bendori S, Gophna U. Menaquinone and iron are essential for complex colony development in *Bacillus subtilis*. *PLoS One* 2013;**8**:e79488.
59. Arnaouteli S, Bamford NC, Stanley-Wall NR *et al.* *Bacillus subtilis* biofilm formation and social interactions. *Nat Rev Microbiol* 2021;**19**:600–14.
60. Toska J, Ho BT, Mekalanos JJ. Exopolysaccharide protects *Vibrio cholerae* from exogenous attacks by the type 6 secretion system. *Proc Natl Acad Sci U S A* 2018;**115**:7997–8002.
61. Rosenberg G, Steinberg N, Oppenheimer-Shaanan Y *et al.* Not so simple, not so subtle: the interspecies competition between *Bacillus simplex* and *Bacillus subtilis* and its impact on the evolution of biofilms. *NPJ Biofilms Microbiomes* 2016;**2**:15027.
62. Lloyd DP, Allen RJ. Competition for space during bacterial colonization of a surface. *J R Soc Interface* 2015;**12**:0608.
63. Jautzus T, van Gestel J, Kovács ÁT. Complex extracellular biology drives surface competition during colony expansion in *Bacillus subtilis*. *ISME J* 2022;**16**:2320–8.
64. Frangipani E, Visaggio D, Heeb S *et al.* The Gac/Rsm and cyclic-di-GMP signalling networks coordinately regulate iron uptake in *Pseudomonas aeruginosa*. *Environ Microbiol* 2014;**16**:676–88.
65. Peng J, Chen G, Xu X *et al.* Iron facilitates the RetS-Gac-Rsm cascade to inversely regulate protease IV (piv) expression via the sigma factor PvdS in *pseudomonas aeruginosa*. *Environ Microbiol* 2020;**22**:5402–13.
66. Zhang B, Zhang Y, Liang F *et al.* An extract produced by *Bacillus* sp. BR3 influences the function of the GacS/GacA two-component system in *Pseudomonas syringae* pv. *Tomato* DC3000. *Front Microbiol* 2005;**2019**:10.
67. Sobrero PM, Valverde C. Comparative genomics and evolutionary analysis of RNA-binding proteins of the CsrA family in the genus *Pseudomonas*. *Front Mol Biosci* 2020;**7**:127.
68. Lapouge K, Schubert M, Allain FHT *et al.* Gac/Rsm signal transduction pathway of γ-proteobacteria: from RNA recognition to regulation of social behaviour. *Mol Microbiol* 2008;**67**:241–53.
69. Wang BX, Wheeler KM, Cady KC *et al.* Mucin glycans signal through the sensor kinase RetS to inhibit virulence-associated traits in *Pseudomonas aeruginosa*. *Curr Biol* 2021;**31**:90–102.
70. Broder UN, Jaeger T, Jenal U. LadS is a calcium-responsive kinase that induces acute-to-chronic virulence switch in *Pseudomonas aeruginosa*. *Nat Microbiol* 2016;**2**:16184.
71. Humair B, González N, Mossialos D *et al.* Temperature-responsive sensing regulates biocontrol factor expression in *Pseudomonas fluorescens* CHA0. *ISME J* 2009;**3**:955–65.
72. Oliveira F, Rohde H, Vilanova M *et al.* The emerging role of iron acquisition in biofilm-associated infections. *Trends Microbiol* 2021;**29**:772–5.
73. Loper JE, Buyer JS. Siderophores in microbial interactions on plant surfaces. *Mol Plant-Microbe Interact* 1991;**4**:5–13.
74. Raaijmakers JM, Van Der Sluis L, Koster M *et al.* Utilization of heterologous siderophores and rhizosphere competence of fluorescent *Pseudomonas* spp. *Can J Microbiol* 1995;**41**:126–35.
75. Yu X, Ai C, Xin L *et al.* The siderophore-producing bacterium, *Bacillus subtilis* CAS15, has a biocontrol effect on Fusarium wilt and promotes the growth of pepper. *Eur J Soil Biol* 2011;**47**:138–45.
76. Chamberlain SA, Bronstein JL, Rudgers JA. How context dependent are species interactions? *Ecol Lett* 2014;**17**:881–90.
77. Zeriouh H, de Vicente A, Pérez-García A *et al.* Surfactin triggers biofilm formation of *Bacillus subtilis* in melon phylloplane and contributes to the biocontrol activity. *Environ Microbiol* 2014;**16**: 2196–211.
78. Palmer A, Phapale P, Chernyavsky I *et al.* FDR-controlled metabolite annotation for high-resolution imaging mass spectrometry. *Nat Methods* 2016;**14**:57–60.